

# Quantum control and entanglement in a chemical compass

Jianming Cai, Gian Giacomo Guerreschi, and Hans J. Briegel

<sup>1</sup>*Institut für Quantenoptik und Quanteninformation der Österreichischen Akademie der Wissenschaften, Innsbruck, Austria*

<sup>2</sup>*Institut für Theoretische Physik, Universität Innsbruck, Technikerstraße 25, A-6020 Innsbruck, Austria*

(Dated: June 7, 2018)

The radical pair mechanism is one of the two main hypotheses to explain the navigability of animals in weak magnetic fields, enabling e.g. birds to see the Earth's magnetic field. We show how quantum control can be used to either enhance or reduce the performance of such a chemical compass, providing a route to further test this hypothesis experimentally. We investigate the dynamics of quantum entanglement in this model, and demonstrate intriguing connections between radical-pair entanglement and the magnetic field sensitivity of the compass. The nature of the nuclear-spin environment plays an essential role for the observed effects.

*Introduction.*— People believe that many species, including birds, insects and mammals, use the Earth's magnetic field for orientation and navigation [1, 2, 3, 4, 5]. Two main hypotheses have been proposed: a magnetite-based mechanism and a radical pair biochemical reaction mechanism. Since the radical pair mechanism (RPM) was first proposed in pioneering work by Schulten *et al.* [6], a magnetic-compass model for migratory birds, based on such a mechanism [7] has been widely studied. Evidence suggests that the RPM is indeed linked to the avian magnetoception [4, 5]. It was recently demonstrated that a photochemical reaction can indeed act as a magnetic compass even in a magnetic field as weak as the geomagnetic field [8]. Furthermore, a class of photoreceptor signalling proteins have been identified to mediate the light-dependent magneto-sensitivity in birds and fruit flies [9, 10, 11]. The other interest in RPM comes from the increasing concern on how weak environmental electromagnetic fields will induce health effects [12, 13].

The underlying mechanism in such a chemical compass is clearly of quantum mechanical nature. However, the detailed role of quantum interactions, giving rise to entanglement and (de-)coherence, are little understood. On the other hand, one can observe growing interest in the role of quantum mechanics for biological processes in general [14, 15, 16, 17, 18, 19, 20], and specifically for the efficiency of energy transfer in photosynthesis [21, 22, 23, 24, 25]. A deeper understanding of the role of quantum mechanics in biology will eventually come along with the ability to control biological processes at the level of individual molecules. In physics, various kinds of quantum control techniques have been developed, specifically in the field of quantum information processing and quantum metrology [26, 27, 28, 29, 30, 31, 32, 33, 34, 35]. The question thus naturally arises to what extent these or similar techniques could be applied to test and refine certain biophysical hypotheses, such as the chemical compass model for animal magnetoception? Can we use quantum technologies that have primarily been developed to control man-made microscopic systems, to influence the behavior of living things — e.g. birds and fruit flies — in a detectable way?

In this paper, aiming at the above questions, we will revisit the chemical compass model using techniques from quantum information. We will investigate the quantum dynamics of a radical pair reaction, and how entanglement between two electron spins in a radical pair evolves during the reaction. We will compare the roles of entanglement and mere classical correlations (arising e.g. from fast de-coherence) for the magnetic-field sensitivity and show how these cases could be distinguished experimentally. By using tools from quantum entanglement theory, we propose a method to estimate the lower bound of entanglement from the experimentally accessible information. We find that quantum coherence and entanglement seem to be necessary for a chemical compass to function properly (compared with purely classical correlations); however, it is really the decay of the entanglement due to de-coherence that plays the essential role. If one tries to promote coherence during the reaction, as people have done for quantum information processing, the chemical compass may no longer work. Quantum control techniques could thus be used to test and refine the chemical compass model, by studying either specific chemical reactions or, more directly, the behavior of animals under the influence of weak (and harmless) magnetic control fields, similar as in the experiments of Wiltshko *et al.* [4, 5].

*Radical pair mechanism.*— We consider a photochemical reaction that starts from the light activation of a photoreceptor, followed by an electron transfer process; two unpaired electrons in a spin-correlated electronic singlet state are then carried by a radical pair. The electron spin relaxation time scale resulting from the molecular motions is considerably longer than the radical pair reaction time. The effective environment of a radical pair thus mainly consists of their individual surrounding nuclei. Without loss of generality, we assume that the external magnetic field points in the  $\hat{z}$  direction. The Hamiltonian of a radical pair is [36] of the form

$$H = \sum_{k=1,2} H_c^{(k)} = -\gamma_e B \sum_k S_z^{(k)} + \sum_{k,j} \lambda_{k,j} \vec{S}^{(k)} \cdot \vec{I}^{(k_j)} \quad (1)$$

where  $\gamma_e = -g_e \mu_B$  is the electron gyromagnetic ratio, and  $\vec{S}^{(k)}$ ,  $\vec{I}^{(k_j)}$  represent the electron and nuclear

spin operators respectively. The nuclear Zeeman interactions are negligible as the gyromagnetic ratio  $\gamma$  for a nucleus is much smaller than  $\gamma_e$ . For simplicity, we neglect the anisotropic hyperfine interactions, the nucleus-nucleus and electron-electron spin exchange interactions [36]. We remark that our general arguments hold even when taking these extra interactions into account, specifically when considering anisotropic interactions that are relevant for the detection of magnetic field directions.

The initial state of a radical pair is assumed to be the singlet state  $|\mathbb{S}\rangle = \frac{1}{\sqrt{2}}(|\uparrow\downarrow\rangle - |\downarrow\uparrow\rangle)$ , which subsequently suffers from de-coherence through the hyperfine interactions with the environmental nuclear spins. The electron-hole recombination of the radical pair goes through different channels dependent on the electron-spin state (singlet or triplet). In particular, the yield of products formed by the reaction of singlet radical pairs can be calculated as [36]

$$\Phi(t) = \int_0^t r_c(t) f_s(t) dt \quad (2)$$

where  $r_c(t)$  is the radical re-encounter probability distribution, and  $f(t) = \langle \mathbb{S} | \rho_s(t) | \mathbb{S} \rangle$  is the fidelity between the electron spin state  $\rho_s(t)$  at time  $t$  and the singlet state. The ultimate activation yield is thus  $\Phi = \Phi(t \rightarrow \infty)$ . It is believed that the activation yield  $\Phi$  in cryptochrome does affect the visual function of animals [10].

*Dynamics of electron spins.*— We note that the Hamiltonian (1) for RPM has been extensively investigated in the field of quantum computation from different aspects [26, 27, 28, 29, 30, 31, 32, 33, 34, 35], most of which aim at protecting the coherence of electron spins from their surrounding nuclei.

For each of the central electron spins, the dynamics depends on the state of the surrounding environmental spins. We assume that the nuclear spins surrounding each electron are initially in a unpolarized state  $\rho_b(0) = \bigotimes_j \mathbb{I}_j/d_j$ , where  $d_j$  is the dimension of the  $j$ th nuclear spin, as the energy of the interaction between the nuclei is much smaller than the thermal energy. The density matrix of the central spin at time  $t$  can then be described by a completely positive map as

$$\rho \rightarrow \mathcal{M}_t[\rho] = W_t \left( \left[ \sum_{m=0}^3 p_m(t) \sigma_m \rho \sigma_m \right] \right) W_t^\dagger \quad (3)$$

where  $\sigma_0 = \mathbb{I}$ ,  $\sigma_1 = 2S_x$ ,  $\sigma_2 = 2S_y$ ,  $\sigma_3 = 2S_z$ ,  $W_t = \text{diag}(e^{i\phi_t}, e^{-i\phi_t})$  is a phase operator, and  $p_0(t) = (a_t + b_t)/2$ ,  $p_1(t) = p_2(t) = (1 - a_t)/2$ ,  $p_3(t) = (a_t - b_t)/2$  depend on two functions  $a_t$  and  $b_t$ .

The spin state of a radical pair evolves from the singlet state  $\mathcal{P}_s = |\mathbb{S}\rangle\langle\mathbb{S}|$  into the mixture

$$\rho_s(t) = \mathcal{M}_t^{(1)} \otimes \mathcal{M}_t^{(2)}[\mathcal{P}_s] \quad (4)$$

As an illustration, we have considered the photochemical reaction of pyrene (Py- $h_{10}$ ) and N,N-dimethylaniline

(DMA- $h_{11}$ ). The radical Py- $h_{10}$  has ten spin- $\frac{1}{2}$  surrounding nuclei with the hyperfine coupling constants  $\lambda_{j_1}^{(1)} = 0.481$  mT ( $4 \times \text{H}$ ),  $\lambda_{j_2}^{(1)} = 0.212$  mT ( $4 \times \text{H}$ ),  $\lambda_{j_3}^{(1)} = 0.103$  mT ( $2 \times \text{H}$ ) [37]. And the radical DMA- $h_{11}$  is mainly coupled with seven spin- $\frac{1}{2}$  nuclei with  $\lambda_{j_1}^{(2)} = 1.180$  mT ( $6 \times \text{H}$ ),  $\lambda_{j_2}^{(2)} = 0.520$  mT ( $1 \times \text{H}$ ), and one spin-1 nucleus with  $\lambda_{j_3}^{(2)} = 1.100$  mT ( $1 \times \text{N}$ ) [38]. We have simulated the full quantum dynamics of the combined system of electron spins and nuclear spins, by employing the Chebyshev polynomial expansion method [39] to calculate the evolution operator  $U_c^{(k)}(t) = e^{-iH_c^{(k)}t}$ , which can be expressed as  $U_c^{(k)}(t) = \sum_{\mu,\nu} |\mu\rangle\langle\nu| \otimes U_{\mu\nu}^{(k)}(t)$ . In this way, we have obtained the parameters  $a_t$ ,  $b_t$  and  $\phi_t$  in Eq. (3).

*Magnetic field sensitivity under quantum control.*— The magnetic field sensitivity  $\Lambda$  of a chemical compass can be characterized by the first derivative of the activation yield with respect to the magnetic field [40],

$$\Lambda(B) = \frac{\partial \Phi}{\partial B} \quad (5)$$

We note that the singlet state  $|\mathbb{S}\rangle$  and the triplet states  $|\mathbb{T}_0\rangle$ ,  $|\mathbb{T}_\pm\rangle$  are the eigenstates of the free Hamiltonian of the two central electron spins,  $H_s = -\gamma_e B \sum_k S_z^{(k)}$ . The hyperfine interactions induce both pure dephasing (from  $S_z I_z$ ), which leads to the transitions  $|\mathbb{S}\rangle \leftrightarrow |\mathbb{T}_0\rangle$ , and spin flip processes (from  $S_x I_x$ ,  $S_y I_y$ ), which leads to  $|\mathbb{S}\rangle \leftrightarrow |\mathbb{T}_\pm\rangle$  and  $|\mathbb{T}_0\rangle \leftrightarrow |\mathbb{T}_\pm\rangle$ . The magnetic field changes the energies of  $|\mathbb{T}_\pm\rangle$ , thereby affecting the singlet-triplet inter conversion. By using an exponential model as an example for the re-encounter probability distribution, i.e.  $r_c(t) = ke^{-kt}$  with  $k$  the recombination rate constant [36], we plot in Fig. 1 the magnetic field sensitivity  $\Lambda$  as a function of  $B$ . Our numerical simulation qualitatively agrees well with the experimental results in [40].

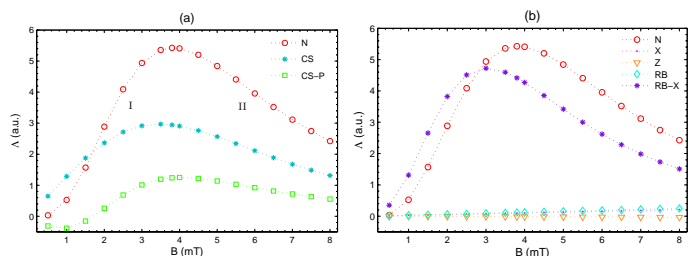


Figure 1: (Color online) Magnetic field sensitivity  $\Lambda$  of a radical pair reaction [Py- $h_{10}^-$  DMA- $h_{11}^+$ ] as a function of the magnetic field  $B$ . (a) N: Singlet initial state; CS: Classically correlated initial state; CS-P: applying a  $\frac{\pi}{2}$  X pulse on the classically correlated initial state. (b) N: Singlet initial states; X: under X control; Z: under Z control; RB (RB-X): periodically re-directional magnetic field without (with) X control. The recombination rate constant is  $k = 5.8 \times 10^8 \text{ s}^{-1}$  [40], and the control time is  $\tau = 0.5 \text{ ns}$ .

We have assumed, as is usually done, that the radical pair starts in a perfect singlet state, i.e. that quan-

tum coherence is fully maintained during the pair creation and electron transfer. One might question this assumption and consider the possibility that (e.g. due to dephasing during the electron transfer) coherence is diminished. Is quantum entanglement thus really necessary for the compass to work? Or could it be explained by mere classical correlations? To obtain some insight into the role of coherence in the RPM, we have assumed an extreme case, where coherence is completely lost during the electron transport process. The initial state after separation of the electrons is then a classical mixture  $\rho_s(0) = (|\uparrow\downarrow\rangle\langle\uparrow\downarrow| + |\downarrow\uparrow\rangle\langle\downarrow\uparrow|)/2$  which contains strict classical correlations, but no entanglement. From Fig. 1(a), we can see that a hypothetical compass working with such an initial state, would have a magnetic field sensitivity that is smaller (larger) than the singlet state for values of  $B$  larger (smaller) than 2mT. This should be accessible to experimental investigation. While it may be difficult to distinguish the predictions of the quantum/classical model from absolute values of  $\Lambda$ , one could e.g. measure the effect of an applied magnetic control field. By noting that the singlet is invariant under rotations  $\mathcal{R} \otimes \mathcal{R}|\mathbb{S}\rangle = |\mathbb{S}\rangle$ , for  $\forall \mathcal{R} \in \mathcal{SU}(2)$ , we propose to apply a  $\frac{\pi}{2}$  pulse along the  $\hat{x}$  direction as the reaction starts. This could be achievable by using the state-of-the-art femtosecond laser techniques [22]. The magnetic field sensitivity for an initial singlet state remains unchanged, whereas for an initial classical mixture (after the pulse) it is much more suppressed, see Fig. 1(a). The basic idea is that the classical mixture can be written as  $\rho_s(0) = (|\mathbb{S}\rangle\langle\mathbb{S}| + |\mathbb{T}_0\rangle\langle\mathbb{T}_0|)/2$ , and a  $\frac{\pi}{2}$ - $X$  pulse changes the population of  $|\mathbb{T}_0\rangle$  to  $|\mathbb{T}_\pm\rangle$ . Thus, even though the magnetic field affects (due to Zeeman splitting within the triplet space) the transitions between  $|\mathbb{T}_0\rangle$  and the triplet states  $|\mathbb{T}_\pm\rangle$ , due to the hyperfine interactions, the initial population of these levels will partially cancel effects of the inter-conversion and suppress the magnetic field sensitivity.

From the comparison of the quantum and classical case in Fig. 1(a), one might expect that increasing the quantum coherence would help to increase the optimal magnetic-field sensitivity, as is the case e.g. in a magnetometer using NV centers in diamond [41, 42]. Interestingly, this turns out not to be true.

A variety of quantum control techniques have been invented for the dynamical decoupling of electron spins from the nuclear spin bath, in order to achieve longer coherence times and to implement quantum computation, e.g. see [26, 27, 28, 29, 30]. Two simple examples of control sequences consist in periodically applying a  $\pi$  pulse at times  $t = m\tau$ , either along the  $\hat{x}$  or the  $\hat{z}$  direction.

Based on the average Hamiltonian theory and the Magnus expansion [43], one can write the time evolution operator under quantum control operations as  $U(t) = e^{-i\bar{H}t} = e^{-i(\bar{H}^{(1)} + \bar{H}^{(2)} + \dots)t}$ , where  $\bar{H}$  is the effective Hamiltonian. For the  $X$  control, to the first or-

der in  $\tau$ , we have  $\bar{H}_X^{(1)} = \frac{1}{2} \sum_k [H^{(k)} + \sigma_1^{(k)} H^{(k)} \sigma_1^{(k)}] = \sum_{k,j} \lambda_{k,j} S_x^{(k)} I_x^{(k_j)}$ . Thus, the hyperfine interactions along the transverse direction are dynamically eliminated. This indeed is helpful to prolong the coherence time, see Fig. 3. However, the effect of the magnetic field is unfortunately removed, too. Thus, even though coherence is enhanced, the magnetic field sensitivity of the chemical compass is lost, as can be seen in Fig. 1(b). Similarly, for the  $Z$  control, the first order effective Hamiltonian is  $\bar{H}_Z^{(1)} = -\gamma_e B \sum_k S_z^{(k)} + \sum_{k,j} \lambda_{k,j} S_z^{(k)} I_z^{(k_j)}$ . This seems to be favorable, as we now dynamically decouple the  $xx$  and  $yy$  hyperfine interactions, while keeping the magnetic-field dependent Zeeman interactions. Nevertheless, the magnetic field sensitivity is greatly suppressed, see Fig. 1(b). For a more detailed explanation, we refer to the Appendix.

We can show that, if one applies more general decoupling protocols to promote quantum coherence in a chemical compass model, its magnetic-field sensitivity will generally be reduced (see Appendix). This is also true for more general situations, e.g. including electron-electron and nucleus-nucleus spin exchange interactions. It is thus the decay of coherence, rather than coherence itself, that plays an essential role for the magnetic-field detection. (This is different from magnetometers using e.g. NV-centers in diamond [41]).

The effect of quantum control depends, however, on the context. To demonstrate a potentially positive effect of quantum control on the dynamics of a chemical compass, we assume a situation where the magnetic field changes its direction periodically, that is

$$B(t) = (-1)^m B \quad \text{for } t \in [m\tau, (m+1)\tau] \quad (6)$$

The first-order effective Hamiltonian is  $\bar{H}_{RB}^{(1)} = \sum_{k,j} \lambda_{k,j} \vec{S}^{(k)} \cdot \vec{I}^{(k_j)}$ , with no magnetic-field dependent term surviving. In other words, if one would design an experiment with animals that use a chemical compass to sense the magnetic field, into such a specific environment, they will lose their orientability via magnetoception, similar as in the experiments reported in [4]. However, if we now apply  $\pi$ - $X$  pulses at time  $t = m\tau$ , the chemical compass can recover its function, see Fig. 1(b), as the average effective Hamiltonian has changed to  $\bar{H}_{RB-X}^{(1)} = -\gamma_e B \sum_k S_z^{(k)} + \sum_{k,j} \lambda_{k,j} S_x^{(k)} I_x^{(k_j)}$ . The residual  $xx$  hyperfine interactions induce transitions between  $|\mathbb{S}\rangle$  and  $|\mathbb{T}_\pm\rangle$ , the energy levels of which are affected by the magnetic field.

For the effects discussed so far, the nuclear spin environment (similar to a spin bath [44]) plays an essential role. This can be seen by comparing it with a hypothetical reference model of a bosonic thermal bath at room temperature, for which most of the present results would be washed out (see Appendix). Similarly, the entanglement dynamics discussed in the next section is strongly connected to the nature and finite size of the spin envi-

ronment.

*Entanglement and magnetic field sensitivity.*— Since entanglement obviously plays a role in the RPM scheme (i.e. beyond mere classical correlations), we have studied its dynamics and its quantitative connection to the magnetic field sensitivity. Similar to the activation yield, we define  $\Phi_E = \int_0^\infty r_c(t)E(t)dt$ , where  $E(t)$  is a measure of entanglement between the two electron spins at time  $t$ , to quantify the effective amount of entanglement that is present in the active radical pairs during the reaction. The corresponding first derivative with respect to the magnetic field,  $\Lambda_E = \partial\Phi_E/\partial B$ , quantifies how sensitive this effective entanglement is with respect to variations of the magnetic field.

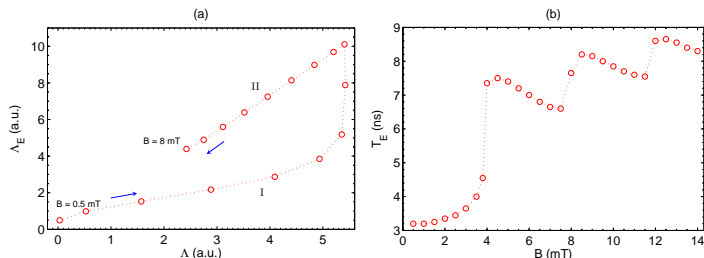


Figure 2: (Color online) (a) Sensitivity of effective entanglement  $\Lambda_E$  vs. sensitivity of singlet yield  $\Lambda$  in a radical pair reaction [Py- $h_{10}^-$  DMA- $h_{11}^+$ ]. The recombination rate constant is  $k = 5.8 \times 10^8 s^{-1}$ . The blue arrows indicate variation of  $\Lambda_E$  and  $\Lambda$  when the magnetic field changes from  $B = 0.5$  mT to  $B = 8$  mT. (b) Discontinuity of the lifetime of entanglement  $T_E$  as a function of  $B$ .

In Fig. 2(a), we see that both in the region I of relatively low magnetic fields, i.e. before  $\Lambda$  reaches its maximum value, and in the region of II,  $\Lambda_E$  and  $\Lambda$  are correlated, displaying a strictly monotonic relation but with different linear ratios. This result is remarkable insofar as that the lifetime of entanglement is much shorter than the reaction time  $T_r$ , i.e. the time it takes for the value of  $\Lambda(B, t) = \partial\Phi(t)/\partial B$  to saturate, in particular in the region of I (see Appendix).

As we can see in Fig. 1, the second derivative of  $\Lambda$  with respect to the magnetic field  $B$  changes its sign, per definition, at the crossing between the regions of I and II. At the same time, it can be seen from Fig. 2(a) that  $\Lambda_E$  changes dramatically in this region. This step-like behavior relates to the discontinuity of the life-time of the entanglement [45, 46]  $T_E = \max\{t|E(t) > 0\}$  as the magnetic field increases, see Fig. 2(b). In the region of I,  $T_E$  is much shorter than the reaction time  $T_r$ , while it jumps to a larger value comparable with  $T_r$  during the crossover from the region of I to II. When we further increase the magnetic field,  $T_E$  exhibits more kinks but with less increment. These kinks originate in the finite size of the nuclear spin environment, and the fact that different values of  $B$  result in different mixtures of singlet and triplet states with different lifetime of entanglement.

*Estimation of entanglement.*— As entanglement obviously exists and seems to play a subtle role in the radical pair reaction, it is natural to address the question how it could be estimated from experimentally accessible information. This problem is certainly non trivial. There are many known methods to detect entanglement in well controllable and separated quantum systems (e.g. by addressing electron spins and performing quantum state tomography). However, it is not clear how to accomplish a similar task in a chemical reaction in solution.

Suppose one can monitor the activation yield  $\Phi(t)$  and that the radical pair re-encounter probability  $r_c(t)$  [40] is known for a specific reaction. From this, we can infer not only the singlet fidelity  $f_s(t)$ , but also the best lower bound of entanglement as in [47, 48],  $\varepsilon(t) = \inf_\rho\{E(\rho)|\text{Tr}(\rho\mathcal{P}_s) = f_s(t)\}$ , where  $E(\rho)$  is chosen to be the entanglement measure of concurrence [49]. For the case of two qubits, one finds that the best lower bound is given by  $\varepsilon(t) = \max\{0, 2f_s(t) - 1\}$ . In Fig. 3, we compare this lower bound with the exact values of the entanglement from numerical simulations, finding good (even though not perfect) agreement, see Appendix. This method could thus provide a way to experimentally estimate the amount of entanglement in the biochemical reaction of the RPM.

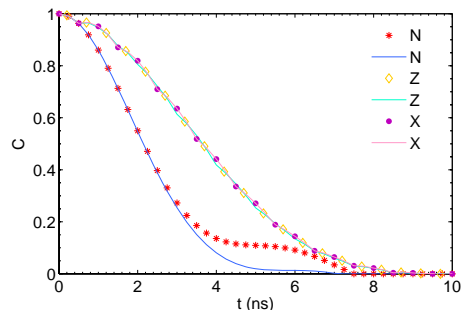


Figure 3: (Color online) Decay of the entanglement in a radical pair reaction [Py- $h_{10}^-$  DMA- $h_{11}^+$ ] under different types of quantum control: (N) without control; (Z) under Z control, (X) under X control. The curves are the estimated best lower bounds from the singlet fidelity, the symbols denote the values from numerical simulation. The magnetic field is  $B = 4.5$  mT, and the control time is  $\tau = 0.5$  ns.

*Summary and outlook.*— We have demonstrated how quantum control can influence the function of a chemical compass, and thus potentially affect the behavior of certain animals. Our results could be extended to probe and control biological functions with state-of-art quantum technologies. We have also investigated the evolution of entanglement in the chemical compass model of avian magnetoreception, and found an interesting connection between the entanglement lifetime and the magnetic field sensitivity. The (nature of the) nuclear spin environment plays thereby an essential role. As a bio-mimetic application of practical interest, it would be interesting to

explore the possibility of simulating a radical-pair mechanism in more controllable quantum systems, such as NV centers in diamond [41, 42, 50], to design an ultra-high fidelity sensor for the detection of weak fields or forces [51].

*Acknowledgements.*— We are grateful for the support from the FWF (J.M.C. through Lise Meitner Program, SFB-FoQuS) and the European Union (QICS, SCALA).

- 
- [1] S. Johnsen, and K. J. Lohmann, *The physics and neurobiology of magnetoreception*, Nature Rev. Neurosci. **6**, 703 (2005).
- [2] H. Burda, S. Begall, J. Červený, J. Neef, and P. Němec, *Extremely low-frequency electromagnetic fields disrupt magnetic alignment of ruminants*, Proc. Natl. Acad. Sci. Advance online, doi: 10.1073/pnas.0811194106 (2009).
- [3] C. T. Rodgers and P. J. Hore, *Chemical magnetoreception in birds: The radical pair mechanism*, Proc. Natl. Acad. Sci. **106**, 353 (2009).
- [4] T. Ritz, P. Thalau, J. B. Phillips, R. Wiltschko, and W. Wiltschko, *Resonance effects indicate a radical-pair mechanism for avian magnetic compass*, Nature. **429**, 177 (2004).
- [5] R. Wiltschko, and W. Wiltschko, *Magnetoreception*, Bioessays. **28**, 157 (2006).
- [6] K. Schulten, c. E. Swenberg, and A. Weller, *A biomagnetic sensory mechanism based on magnetic field modulated coherent electron spin motion*, Z. Phys. Chem. **NF111**, 1 (1978).
- [7] T. Ritz, S. Adem, and K. Schulten, *A model for photoreceptor-based magnetoreception in birds*, Biophys. J. **78**, 707 (2000).
- [8] K. Maeda and K. B. Henbest, F. Cintolesi, I. Kuprov, C. T. Rodgers, P. A. Liddell, D. Gust, C. R. Timmel and P. J. Hore, *Chemical compass model of avian magnetoreception*, Nature. **453**, 387 (2008).
- [9] M. P. Galland, T. Ritz, R. Wilschko, and W. Wilschko, *Magnetic intensity affects cryptochrome-dependent response in Arabidopsis thaliana*, Planta. **225**, 615 (2006).
- [10] I. A. Solov'yov, D. E. Changler, and K. Schulten, *Magnetic field effects in Arabidopsis thaliana Cryptochrome-1*, Biophys. J. **92**, 2711 (2007).
- [11] R. J. Gegeer, A. Casselman, S. Waddell, and S. M. Reppert, *Cryptochrome mediates light-dependent magnetosensitivity in Drosophila*, Nature **454**, 1014 (2008).
- [12] B. Brocklehurst, K. A. McLauchlan, *Free radical mechanism for the effects of environmental electromagnetic fields on biological systems*, Int. J. Radiat. Biol. **69**, 3 (1996).
- [13] B. Brocklehurst, *Magnetic fields and radical reactions: recent developments and their role in nature*, Chem. Soc. Rev. **31**, 301 (2002).
- [14] D. Abbott, P. C. W. Davies, A. K. Pati, (eds.) *Quantum Aspects of Life* (World Scientific, Singapore, 2008).
- [15] H. J. Briegel, S. Popescu, *Entanglement and intramolecular cooling in biological systems? – A quantum thermodynamic perspective*, arxiv: 0806.4552.
- [16] J.-M. Cai, S. Popescu, H. J. Briegel, *Dynamical entanglement in oscillating molecules*, arXiv:0809.4906.
- [17] J. Gilmore, R. H. McKenzie, *Spin-boson models for quantum decoherence of electronic excitations of biomolecules and quantum dots in a solvent*, J. Phys: Cond. Mat. **17**, 1735 (2005).
- [18] J. Gilmore, R. H. McKenzie, *Quantum dynamics of electronic excitations in biomolecular chromophores: Role of the protein environment and solvent*, J. Phys. Chem. A **112**, 2162 (2008).
- [19] S. Lloyd, *A quantum of natural selection*, Nature Physics **5**, 164 (2009).
- [20] W. H. Zurek, *Quantum Darwinism*, Nature Physics **5**, 181 (2009).
- [21] G. S. Engel, T. R. Calhoun, E. L. Read, T. K. Ahn, T. Mancal, Y. C. Cheng, R. E. Blankenship, G. R. Fleming, *Evidence for wavelike energy transfer through quantum coherence in photosynthetic systems*, Nature **446**, 782 (2007).
- [22] H. Lee, Y.-C. Cheng, and G. R. Fleming, *Coherence Dynamics in Photosynthesis: Protein Protection of Excitonic Coherence*, Science **316**, 1462(2007).
- [23] M. Mohseni, P. Rebentrost, S. Lloyd, A. Aspuru-Guzik, *Environment-assisted quantum walks in photosynthetic energy transfer*, J. Chem. Phys. **129**, 174106 (2008).
- [24] M. B. Plenio, S. F. Huelga, *Dephasing assisted transport: Quantum networks and biomolecules*, New J. Phys. **10**, 113019 (2008).
- [25] M. Sarovar and A. Ishizaki and G. R. Fleming and K. Birgitta Whaley, *Quantum entanglement in photosynthetic light harvesting complexes*, arXiv: 0905.3787.
- [26] L. Viola, E. Knill, and S. Lloyd, *Dynamical decoupling of open quantum systems*, Phys. Rev. Lett. **82**, 2417 (1999).
- [27] R. de Sousa, N. Shenvi, and K. B. Whaley, *Qubit coherence control in a nuclear spin bath*, Phys. Rev. B **72**, 045330 (2005).
- [28] W.-X. Zhang, N. P. Konstantinidis, V. V. Dobrovitski, B. N. Harmon, Lea F. Santos, and L. Viola, *Long-time electron spin storage via dynamical suppression of hyperfine-induced decoherence in a quantum dot*, Phys. Rev. B **77**, 125336 (2008)
- [29] Götz S. Uhrig, *Concatenated Control Sequences Based on Optimized Dynamic Decoupling*, Phys. Rev. Lett. **102**, 120502 (2009).
- [30] M. J. Biercuk *et al.*, *Optimized dynamical decoupling in a model quantum memory*, Nature **458**, 996-1000 (2009).
- [31] W. Yang and R.-B. Liu, *Quantum many-body theory of qubit decoherence in a finite-size spin bath*, Phys. Rev. B **78**, 085315 (2008).
- [32] J. Fischer, M. Trif, W. A. Coish, D. Loss, *Spin interactions, relaxation and decoherence in quantum dots*, arXiv:0903.0527.
- [33] L. Cywiński, W. M. Witzel, and S. Das Sarma, *Electron Spin Dephasing due to Hyperfine Interactions with a Nuclear Spin Bath*, Phys. Rev. Lett. **102**, 057601 (2009).
- [34] Igor Žutić and Jaroslav Fabian and S. Das Sarma, *Spintronics: Fundamentals and applications*, Rev. Mod. Phys. **76**, 323 (2004).
- [35] P. Cappellaro, L. Jiang, J. S. Hodges, M. D. Lukin, *Coherence and control of quantum registers based on electronic spin in a nuclear spin bath*, arXiv:0901.0444.
- [36] U. E. Steiner, T. Ulrich, *Magnetic field effects in chemical kinetics and related phenomena*, Chem. Rev. **89**, 51 (1989).
- [37] R. F. Claridge, C. M. Kirk, B. M. Peake, <sup>13</sup>C coupling in the E.S.R. spectrum of the pyrene anion in tetrahydrofu-

- ran, Aust. J. Chem. 1973, 26, 2055 (1973).
- [38] B. G. Pobedimskii, A. L. Buchachenko, M. B. Neiman, Russ. J. Phys. Chem. 42, 748 (1968).
- [39] V. V. Dobrovitski and H. A. De Raedt, *Efficient scheme for numerical simulations of the spin-bath decoherence*, Phys. Rev. E **67**, 056702 (2003).
- [40] C. T. Rodgers, Stuart A. Norman, K.B. Henbest, C. R. Timmel, and P. J. Hore, *Determination of radical re-encounter probability distributions from magnetic field effects on reaction yields*, J. Am. Chem. Soc. **129**, 6746 (2007).
- [41] J. M. Taylor, P. Cappellaro, L. Childress, L. Jiang, D. Budker, P. R. Hemmer, A. Yacoby, R. Walsworth, M. D. Lukin, *High-sensitivity diamond magnetometer with nanoscale resolution*, Nature Physics **4**, 810 - 816 (2008).
- [42] J. R. Maze et al., *Nanoscale magnetic sensing with an individual electronic spin in diamond*, Nature **455**, 644-647 (2008).
- [43] W. Magnus, *On the exponential solution of differential equations for a linear operator*, Communications on Pure and Applied Mathematics, **7**, 649 (1954).
- [44] N. Prokofev, P. Stamp, *Theory of the spin bath*, Rep. Prog. Phys. **63**, 669 (2000).
- [45] W. Dür and H.-J. Briegel, *Stability of Macroscopic Entanglement under Decoherence*, Phys. Rev. Lett. **92**, 180403 (2004).
- [46] T. Yu and J. H. Eberly, *Finite-Time Disentanglement Via Spontaneous Emission*, Phys. Rev. Lett. **93**, 140404 (2004).
- [47] O. Gühne, M. Reimpell, and R. F. Werner, *Estimating Entanglement Measures in Experiments*, Phys. Rev. Lett. **98**, 110502 (2007).
- [48] O. Gühne, M. Reimpell, and R. F. Werner, *Lower bounds on entanglement measures from incomplete information*, Phys. Rev. A **77**, 052317 (2008).
- [49] W. K. Wootters, *Entanglement of Formation of an Arbitrary State of Two Qubits*, Phys. Rev. Lett. **80**, 2245 (1998).
- [50] G. Balasubramanian et al., *Nanoscale imaging magnetometry with diamond spins under ambient conditions*, Nature **455**, 648 (2008).
- [51] J.M. Cai *et al.* unpublished.
- [52] H. P. Breuer, F. Petruccione, *The Theory of Open Quantum Systems* (Oxford University Press, New York, 2002).
- [53] H. J. Briegel, B. G. Englert, *Quantum optical master equations: The use of damping bases*, Phys. Rev. A **47**, 3311-3329 (1993).

## APPENDIX

In this Appendix, we provide more details to support the above results. We first derive the completely positive map as given in Eq. (3) for the dynamics of a central spin coupled to its surrounding nuclear spins. We show that even though entanglement and coherence play an essential role, it is not helpful for a chemical compass to promote its quantum coherence. More details are provided to clarify the connections between quantum entanglement and magnetic field sensitivity. To illustrate the essential role of the (de-phasing) nuclear spin environ-

ment in a chemical compass, we investigate a hypothetical reference model of bosonic thermal bath and compare it with the present results.

*Completely positive map for electron spin dynamics.*— The Hamiltonian for a central unpaired electron spin coupled with a nuclear spin bath is written as

$$H_c = m_b S_z + \sum_k \lambda_k \vec{S} \cdot \vec{I}^{(k)} \quad (7)$$

where  $m_b = -\gamma_e B$ . The presently available theories for

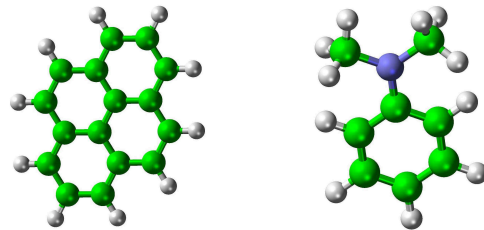


Figure 4: (Color online) Molecular structures for pyrene (Py- $h_{10}$ ) (left) and for N,N-dimethylaniline (DMA- $h_{11}$ ) (right). Green: Carbon; Grey: Hydrogen; Blue: Nitrogen.

the central spin problem usually resort to the perturbation approach, based on certain approximations, e.g. the quasi-static approximation or the limit of large magnetic fields and/or large spin bath polarizations. For our present purpose, these approximations are only of limited use since, in the radical pair mechanism, one is particularly interested in the region of low fields, and the number of most relevant surrounding nuclei is  $\sim 10$ , in contrast with  $\sim 10^5$  in quantum dots. For example, as we can see from the molecular structures displayed in Fig. 4, Py- $h_{10}$  has ten spin- $\frac{1}{2}$  hydrogen nuclei, there are eleven spin- $\frac{1}{2}$  hydrogen nuclei and one spin-1 nitrogen nucleus in DMA- $h_{11}$ , and the nuclear spin of carbon is 0. In our numerical simulations, without loss of essential features, we have considered three groups of equivalent nuclei in each radical that have the largest hyperfine couplings [40].

It is straightforward to show that the total angular momentum of the electron and nuclear spins,  $M_z = S_z + I_z$ , where  $I_z = \sum_k I_z^{(k)}$ , is conserved for the Hamiltonian in Eq. (7), i.e.  $[M_z, H_c] = 0$ . By introducing  $\{|\varphi_n^m\rangle\}$  as the basis of eigenstates of  $I_z$ , i.e.  $I_z|\varphi_n^m\rangle = n|\varphi_n^m\rangle$ , where  $n$  labels the eigenvalues and  $m$  is a degeneracy index, we can express the initial state of the spin bath as  $\rho_b(0) = \bigotimes_k \mathbb{I}_k/d_k = \frac{1}{d} \sum_{n,m} |\varphi_n^m\rangle \langle \varphi_n^m|$ , where  $d = \prod_k d_k$  is the total dimension of all the (relevant) nuclear spins. Thus, under the coherent evolution  $U_c = \exp(-itH_c)$ , the joint state of the central spin and the nuclear spins evolves as

$$|\uparrow\rangle |\varphi_n^m\rangle \rightarrow |\uparrow\rangle |\varphi_{mn}^0\rangle + |\downarrow\rangle |\varphi_{mn}^1\rangle \quad (8)$$

$$|\downarrow\rangle |\varphi_n^m\rangle \rightarrow |\uparrow\rangle |\varphi_{mn}^{-1}\rangle + |\downarrow\rangle |\varphi_{mn}^0\rangle \quad (9)$$

wherein  $|\downarrow\rangle$  and  $\langle\downarrow|$  denote the eigenstates of  $S_z = \hbar/2\sigma_z$ , and  $|\varphi_{mn}^i\rangle$  belongs to the eigenspace of  $I_z$  associated to the eigenvalue  $n+i$ . The fact that the total angular momentum is conserved results in orthogonality relations for the nuclear spin states:

$$|\varphi_{mn}^0\rangle, |\varphi_{mn}^{0'}\rangle \perp |\varphi_{mn}^{-1}\rangle \perp |\varphi_{mn}^1\rangle \quad (10)$$

The inner products of these vectors are zero, as they belong to orthogonal subspaces (or are null vectors).

By recalling the notation  $\frac{1+\sigma_z}{2} = |\uparrow\rangle\langle\uparrow|$ ,  $\frac{1-\sigma_z}{2} = |\downarrow\rangle\langle\downarrow|$ ,  $\sigma_+ = |\uparrow\rangle\langle\downarrow|$ ,  $\sigma_- = |\downarrow\rangle\langle\uparrow|$ , we obtain

$$\begin{aligned} \mu_{0+} &= \text{Tr} \left[ U_c \left( \frac{1+\sigma_z}{2} \otimes \frac{\mathbb{I}}{d} \right) U_c^\dagger (\sigma_+ \otimes \mathbb{I}) \right] \\ &\propto \text{Tr} \left[ U_c \left( \sum_{n,m} |\uparrow\rangle |\varphi_n^m\rangle \langle\varphi_n^m| \langle\uparrow| \right) U_c^\dagger (\sigma_+ \otimes \mathbb{I}) \right] \\ &= \text{Tr} \sum_{n,m} |\varphi_{mn}^1\rangle \langle\varphi_{mn}^0| \\ &= 0 \end{aligned} \quad (11)$$

in which we have used the relation in Eq. (10). In a similar way, one can show that  $\mu_{0-} = \mu_{1\pm} = \mu_{\pm 0} = \mu_{\pm 1} = \mu_{++} = \mu_{--} = 0$ . Moreover, it is easy to verify that

$$\mu_{00} = \mu_{11} = \frac{1}{2} + \frac{1}{4d} \text{Tr} (U_c \sigma_z U_c^\dagger \sigma_z)$$

Thus, the dynamics of the central spin, which is calculated by tracing out its spin bath degrees of freedom as  $\rho_s(t) = \text{Tr}_b \{ e^{-iH_c t} [\rho_s(0) \otimes \rho_b(0)] e^{iH_c t} \}$ , can be explicitly expressed as

$$\begin{aligned} \xi(t) : \quad &|\uparrow\rangle\langle\uparrow| \rightarrow a_t |\uparrow\rangle\langle\uparrow| + (1-a_t) |\downarrow\rangle\langle\downarrow| \\ &|\downarrow\rangle\langle\downarrow| \rightarrow (1-a_t) |\uparrow\rangle\langle\uparrow| + a_t |\downarrow\rangle\langle\downarrow| \\ &|\uparrow\rangle\langle\downarrow| \rightarrow \kappa_t |\uparrow\rangle\langle\downarrow| \\ &|\downarrow\rangle\langle\uparrow| \rightarrow \kappa_t^* |\downarrow\rangle\langle\uparrow| \end{aligned}$$

By writing  $\kappa_t = b_t e^{i2\phi_t}$ , we obtain the completely positive map for the central spin dynamics as in Eq. (3). If we rewrite the evolution operator  $U_c = e^{-itH_c}$  in the form of  $U_c = \sum_{\mu,\nu} |\mu\rangle\langle\nu| \otimes U_{\mu\nu}$ , we get the above dynamic parameters  $a_t = \text{Tr}(U_{00}U_{00}^\dagger)$ , and  $b_t = |\kappa_t|$ ,  $2\phi_t = \arg \kappa_t$  where  $\kappa_t = \text{Tr}(U_{00}U_{11}^\dagger)$ .

*Protecting coherence is not helpful.*— In the magnetometer with the NV centers in diamond, the sensitivity is indeed dependent on the coherence time, i.e. the longer coherence time the better its sensitivity [41, 42]. This however is not the case in a chemical compass model.

As we have described in the main text, for the Z control, we dynamically decouple the xx and yy hyperfine interactions while keeping the magnetic-field dependent Zeeman interactions. Nevertheless, the magnetic field sensitivity is still much suppressed. This phenomenon can be understood as follows. The residual hyperfine

couplings along the longitudinal direction (i.e. zz hyperfine couplings) only induce the transitions between the singlet state  $|\mathbb{S}\rangle$  and one specific triplet state  $|\mathbb{T}_0\rangle$ , while these two eigenstates are degenerate and their energies are independent of the magnetic field. In this case, the singlet-triplet interconversion is actually not influenced by the magnetic field, the effects of which are thus not detectable through the activation yield. We will prove, in the following, that a chemical compass will lose its function, if one uses general dynamical decoupling protocols to promote the electron spin coherence.

Assume that, at time  $t_0$ , the electron spins and surrounding the nuclear spins are in some state  $\rho(t_0) = \rho_0$ . The activation yield during a short time interval  $[t_0, t_0 + \tau]$  is

$$\Phi(t_0, \tau) = \int_{t_0}^{t_0+\tau} r_c(t) f_s(t) dt \quad (12)$$

with the singlet fidelity  $f_s(t)$  as defined after eq. 2. We then write its first derivative with respect to the magnetic field as

$$\Lambda(t_0, \tau) = \frac{\partial \Phi(t_0, t_0 + \tau)}{\partial B} = \int_{t_0}^{t_0+\tau} r_c(t) \frac{\partial f_s(t)}{\partial B} dt$$

which obviously determines the ultimate magnetic field sensitivity as  $\Lambda = \sum_m \Lambda(m\tau, \tau)$  by summing up  $\Lambda(t_0, \tau)$  for all time intervals  $[t_0, t_0 + \tau] = [m\tau, (m+1)\tau]$ ,  $m = 0, 1, 2, \dots$ . The singlet fidelity at time  $t \in [t_0, t_0 + \tau]$  is  $f_s(t) = \text{Tr} (e^{-i\Delta t H} \rho_0 e^{i\Delta t H} \mathcal{P}_s)$  with  $\Delta t = t - t_0$ , and  $H$  is the Hamiltonian of the electron spins together with the nuclear spins as in Eq. (1). By using a perturbation expansions for small  $\Delta t$ , we have

$$e^{-i\Delta t H} = \mathbb{I} - i\Delta t H - \frac{(\Delta t)^2}{2} H^2 + O((\Delta t)^3) \quad (13)$$

which enables us to express the singlet fidelity as follows,

$$\begin{aligned} f_s(t) &= \text{Tr} \left[ \rho_0 \left( \mathcal{P}_s + i\Delta t [H, \mathcal{P}_s] + \frac{(\Delta t)^2}{2} [[H, \mathcal{P}_s], H] \right) \right] \\ &\quad + O(\Delta t^3) \end{aligned} \quad (14)$$

where  $[A, B] = AB - BA$  and  $\{A, B\} = AB + BA$  (see below). Using the properties of the singlet state that  $\frac{\partial H}{\partial B} \mathcal{P}_s = \mathcal{P}_s \frac{\partial H}{\partial B} = 0$ , where  $\frac{\partial H}{\partial B} = -\gamma_e (S_z^{(1)} + S_z^{(2)})$ , the first derivative of  $f_s(t)$  can be written as

$$\begin{aligned} \frac{\partial f_s(t)}{\partial B} &= -\frac{(\Delta t)^2}{2} \text{Tr} \left[ \rho_0 \left( \frac{\partial H}{\partial B} H \mathcal{P}_s + \mathcal{P}_s H \frac{\partial H}{\partial B} \right) \right] \\ &\quad + O((\Delta t)^3) \end{aligned} \quad (15)$$

If  $\rho_0 = \mathcal{P}_s \otimes \frac{\mathbb{I}}{d}$ , one can easily verify that  $\text{Tr} [\rho_0 (\frac{\partial H}{\partial B} H \mathcal{P}_s + \mathcal{P}_s H \frac{\partial H}{\partial B})] = 0$ . Thus, if a dynamical decoupling protocol is to protect the electron spin coherence during the reaction, i.e. keep the spin state close

to the singlet state, we can conclude that  $\partial f_s(t)/\partial B \simeq O((\Delta t)^3)$ , and  $\Lambda(t_0, \tau)$  will be of the fourth order in  $\tau$ , which is an order smaller than the one from other general states. We remark that we do not trivially assume that the system dynamics is frozen by protecting coherence, but the electron spin state does evolve even if it is kept closer to the singlet state under decoupling controls.

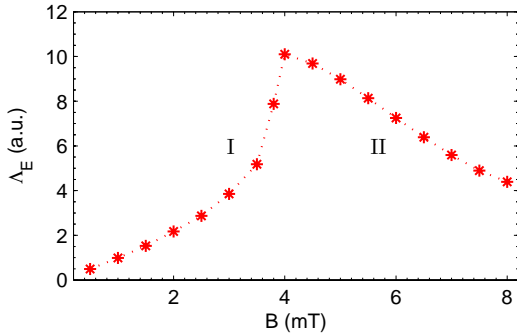


Figure 5: (Color online) Entanglement sensitivity  $\Lambda_E$  of a radical pair reaction  $[\text{Py}-h_{10}^- \text{DMA}-h_{11}^+]$  as a function of the magnetic field  $B$ . The recombination rate constant is  $k = 5.8 \times 10^8 \text{ s}^{-1}$ .

*Entanglement and magnetic field sensitivity.*— Similar to the activation yield, we define the effective entanglement  $\Phi_E$  as follows,

$$\Phi_E = \int_0^\infty r_c(t)E(t)dt \quad (16)$$

It quantifies the amount of entanglement that exists in the active radical pairs during the reaction, and the corresponding first derivative with respect to the magnetic field is

$$\Lambda_E = \frac{\partial \Phi_E}{\partial B} \quad (17)$$

In Fig. 5, we plot  $\Lambda_E$  as a function of  $B$ . It can be seen that,  $\Lambda_E$  changes dramatically during the crossover between the region of I and II. The entanglement yield, however, always increases with the magnetic field. This can be understood from the fact that strong magnetic fields will energetically suppress the relaxation (spin flips) in the longitudinal direction. By this process, the state of the electron pairs changes towards a binary mixture of two entangled states, which is entangled for almost all values of the mixing parameter, resulting in a much larger lifetime of entanglement.

To further illuminate the connection between quantum entanglement and magnetic field sensitivity in a chemical compass, we plot the evolution of entanglement and the value of the accumulated magnetic-field sensitivity  $\Lambda(B, t) = \partial \Phi(t)/\partial B$  as a function of time, for different values of the magnetic field:  $B = 3\text{mT}$ ,  $3.5\text{mT}$ ,  $4\text{mT}$ , and  $4.5\text{mT}$ . The lifetime of entanglement in the region of I is

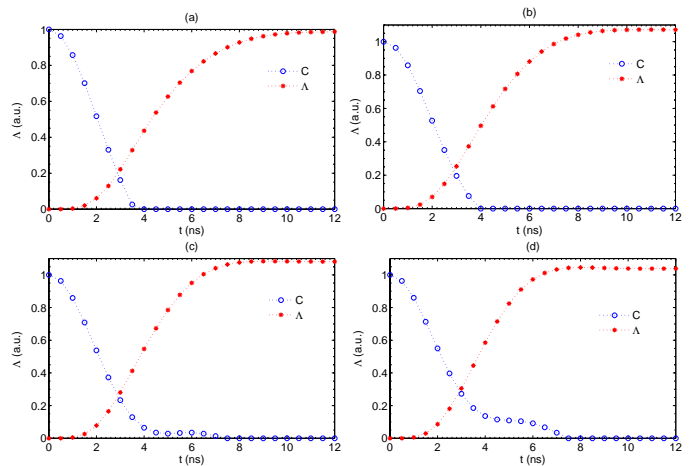


Figure 6: (Color online) Evolution of the (accumulated) magnetic-field sensitivity  $\Lambda(B, t)$  (rescaled) and the entanglement of the radical pair for (a)  $B = 3\text{mT}$ , (b)  $3.5\text{mT}$ , (c)  $4\text{mT}$ , and (d)  $4.5\text{mT}$  in the radical pair reaction  $[\text{Py}-h_{10}^- \text{DMA}-h_{11}^+]$ , as a function of time  $t$ . The recombination rate constant is  $k = 5.8 \times 10^8 \text{ s}^{-1}$ .

about  $T_E = 4 \text{ ns}$ , while  $\Lambda(B, t)$  needs about  $T_r = 10\text{ns}$  to reach its saturate value, see Fig. 6(a-b). We can also explicitly see the jumping feature of  $T_c$  when  $B$  crosses between the regions of I and II, from  $T_E = 4\text{ns}$  to about  $7.3\text{ns}$ , see Fig. 6 (c-d), which gives rise to the steps in Fig. 2(b).

*Reference model of a bosonic heat bath.*— Let us assume that each of the unpaired electron spins is coupled with an independent bosonic heat bath at the same temperature. The dynamics of one central spin would thus be described by the following Lindblad type master equation [52, 53]

$$\frac{\partial}{\partial t} \rho = -\frac{i}{\hbar} [H_c, \rho] + \sum_k (2L_k \rho L_k^\dagger - \rho L_k^\dagger L_k - L_k^\dagger L_k \rho) \quad (18)$$

where  $H_c = m_b S_z$ , with  $m_b = -\gamma_e B$ ,  $L_1 = \sqrt{\gamma s} \sigma_+$  and  $L_2 = \sqrt{\gamma(1-s)} \sigma_-$ . The solution of the above master equation can be represented by a map  $\rho(t) = \overline{\mathcal{M}}_t[\rho(0)]$  which is explicitly expressed as follows

$$\begin{aligned} \overline{\mathcal{M}}_t : \quad & |\uparrow\rangle \langle \uparrow| \rightarrow \alpha_t |\uparrow\rangle \langle \uparrow| + (1 - \alpha_t) |\downarrow\rangle \langle \downarrow| \\ & |\downarrow\rangle \langle \downarrow| \rightarrow (1 - \beta_t) |\uparrow\rangle \langle \uparrow| + \beta_t |\downarrow\rangle \langle \downarrow| \\ & |\uparrow\rangle \langle \downarrow| \rightarrow e^{-i2m_b t} \eta_t |\uparrow\rangle \langle \downarrow| \\ & |\downarrow\rangle \langle \uparrow| \rightarrow e^{i2m_b t} \eta_t |\downarrow\rangle \langle \uparrow| \end{aligned}$$

where  $\alpha_t = (1-s)e^{-2\gamma t} + s$ ,  $\beta_t = se^{-2\gamma t} + (1-s)$  and  $\eta_t = e^{-\gamma t}$ . This map describes spin-exchange interactions with the environment with effective rate  $\gamma$ , and an equilibrium parameter  $s$  that is related to the environment temperature  $T$ . The dependence of  $\gamma$  and  $s$  on  $T$  and the magnetic field  $B$  is given in the following way:  $\gamma = 2m_b \kappa_0 (2\mathcal{N} + 1)$  and  $s = \mathcal{N} / (2\mathcal{N} + 1)$ , where  $\kappa_0$  represents the system-bath coupling strength, and the bosonic



distribution function is  $\mathcal{N} = 1/(e^{\frac{\epsilon_s}{\epsilon_T}} - 1)$  with the system energy scale as  $\epsilon_s = 2\hbar m_b$  and the thermal energy scale as  $\epsilon_T = k_b T$ . Thus we have

$$\frac{1}{s} \frac{\partial s}{\partial B} = -\frac{s}{B} \frac{\epsilon_s}{\epsilon_T} e^{\frac{\epsilon_s}{\epsilon_T}} \quad (19)$$

$$\frac{1}{\gamma} \frac{\partial \gamma}{\partial B} = \frac{1}{B} \left[ 1 - 2 \frac{\epsilon_s}{\epsilon_T} e^{\frac{\epsilon_s}{\epsilon_T}} (e^{2\frac{\epsilon_s}{\epsilon_T}} - 1)^{-1} \right] \quad (20)$$

Since we are interested in the effects of low magnetic fields, for example  $B = 1\text{mT}$ , which corresponds to the thermal energy scale at temperature  $T \simeq 2.69\text{mK}$  which is quite low for biochemical systems. Thus we can naturally assume that  $\frac{\epsilon_s}{\epsilon_T} \ll 1$ , from which it is easy to verify that  $\left| \frac{1}{\gamma} \frac{\partial \gamma}{\partial B} \right| \ll \left| \frac{1}{s} \frac{\partial s}{\partial B} \right|$ , e.g. if  $T = 1\text{K}$  then  $\left| \frac{1}{\gamma} \frac{\partial \gamma}{\partial B} \right|$  is already four orders smaller than  $\left| \frac{1}{s} \frac{\partial s}{\partial B} \right|$ .

The radical pair starts in the singlet state  $|\mathbb{S}\rangle = \frac{1}{\sqrt{2}}(|\uparrow\downarrow\rangle - |\downarrow\uparrow\rangle)$ , and its state evolves as  $\rho_s(t) = \overline{\mathcal{M}}_t^{(1)} \otimes \overline{\mathcal{M}}_t^{(2)}[\mathcal{P}_s]$ . At time  $t$ , the density matrix is of the following form

$$\rho_s(t) = \begin{pmatrix} a & 0 & 0 & 0 \\ 0 & b & c & 0 \\ 0 & c & b & 0 \\ 0 & 0 & 0 & d \end{pmatrix} \quad (21)$$

where  $a = \alpha_t(1 - \beta_t)$ ,  $b = [\alpha_t\beta_t + (1 - \alpha_t)(1 - \beta_t)]/2$ ,  $d = (1 - \alpha_t)\beta_t$ , and  $c = -\eta_t^2/2$ . Thus we can calculate the singlet fidelity  $f_s(t) = \text{Tr}[\rho(t)\mathcal{P}_s] = b - c$  as

$$f_s(t) = \frac{1}{2} [\alpha_t\beta_t + (1 - \alpha_t)(1 - \beta_t) + \eta_t^2]$$

The activation yield for the exponential re-encounter probability model is  $\Phi = \int_0^\infty f_s(t) k e^{-kt} dt$ , i.e.

$$\Phi = \frac{k}{k + 2\gamma} + \frac{8\gamma^2}{(k + 4\gamma)(k + 2\gamma)} s(1 - s)$$

One can verify that under the general conditions we are interested in, the magnitude of the magnetic field sensitivity  $\Lambda$  would increase with the coupling strength  $\kappa_0$ , i.e. the fast thermalization is good in the present context. To achieve the optimal bound of  $\Lambda$ , and illustrate the essential physics, we can assume that  $\gamma$  is much larger than  $k$  (this is different from the real situation where  $\gamma$  is smaller than  $k$ ), which leads to

$$\Lambda \simeq -(1 - 2s) \frac{s^2}{B} \frac{\epsilon_s}{\epsilon_T} e^{\frac{\epsilon_s}{\epsilon_T}} \quad (22)$$

The magnitude of  $\Lambda$  from the bosonic heat bath decreases as the temperature increases. Even at temperature as low as 1 K, it is already significantly smaller than the one from the nuclear spin environment, see Fig. 7. Therefore, we can conclude that the effects of low magnetic

fields will indeed be washed out completely by the thermal fluctuations.

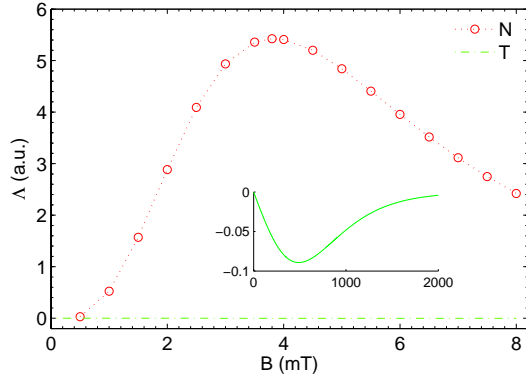


Figure 7: (Color online) Magnetic field sensitivity  $\Lambda$  resulting from the nuclear spin environment ( $N$ ) of the radical pair reaction  $[\text{Py}-h_{10}^- \text{DMA}-h_{11}^+]$ ; and the optimal  $\Lambda$  (achieve when  $\gamma \gg k$ ) from the bosonic heat bath at temperature  $T = 1\text{K}$  (see also Inset for an extended range of parameter) as a function of the magnetic field  $B$ . The recombination rate constant is  $k = 5.8 \times 10^8 \text{s}^{-1}$ .

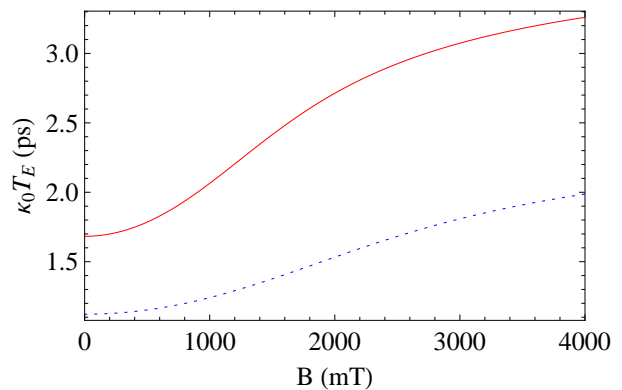


Figure 8: (Color online) Lifetime of entanglement  $\kappa_0 T_E$  as a function of the magnetic field  $B$ . The bath temperature is  $T = 1\text{K}$  (red solid) and  $T = 1.5\text{K}$  (blue dotted).

By calculating  $\partial|\Lambda|/\partial B$ , we find that  $|\Lambda|$  will always grow as the magnetic field becomes stronger, as long as  $\frac{\epsilon_s}{\epsilon_T} \leq \ln(2 + \sqrt{3})$ , which is obviously satisfied in the regions we are interested in. The change of the sign of  $\partial|\Lambda|/\partial B$  happens at  $\frac{\epsilon_s}{\epsilon_T} = \ln(2 + \sqrt{3})$ . At room temperature  $T = 300\text{K}$ , this would correspond to the magnetic field  $B \sim 135\text{T}$ .

The evolution of entanglement as obtained from Eq. (21) is  $E(t) = \max\{0, 2(|c| - (ad)^{1/2})\}$ . In a similar way, one can obtain the lifetime of entanglement, see Fig. 8, which is monotonically increasing with the magnetic field. This is another feature in marked contrast with the nuclear spin environment: The entanglement lifetime is not only much shorter, but there are also no kinks in the lifetime as the magnetic field increases.